

Lithium-bearing minerals under the scanning electron microscope equipped with energy dispersive spectrometry: Challenges, recent advances and prospects



Vincent Thiery ^{a,b,*}, Hasmik Bou Farhat ^{a,b}

^a IMT Nord Europe, Institut Mines-Télécom, Centre for Materials and Processes, F-59000 Lille, France

^b Univ. Lille, Institut Mines-Télécom, LGCgE – Laboratoire de Génie Civil et géoEnvironnement, F-59000 Lille, France

ARTICLE INFO

Editor: Claudia Romano

Keywords:

Lithium bearing minerals
Monte Carlo simulation
Energy dispersive spectroscopy
Backscattered coefficient

ABSTRACT

The challenges of lithium analysis by the means of energy dispersive spectroscopy (EDS) are still present nowadays despite commercially available windowless detectors, which are not widespread. Since scanning electron microscopy (SEM), coupled with EDS, is the most common analytical tool in materials characterization, it is not surprising to observe an increase in the interest of Li analysis within this framework. However, there are still challenges to overcome, namely the choice of adequate analytical conditions as well as an understanding of the material behaviour under the electron gun. The present study illustrates a lepidolite-bearing granite and a spodumene crystal to show the limitations of conventional (i.e. with a window) EDS detector. It is broadened by the calculation of backscattered coefficients for the most common Li-bearing minerals, showing the weak contrasts they display in backscattered images. Monte Carlo simulation of electron-matter interactions within the different minerals show the size of the interaction zone. Finally, a presentation of simulated spectra can guide the user for a better identification of the phases of interest.

1. Introduction

The society is highly dependent on lithium (Bibienne et al., 2020). Current trends in electric cars development will generate high number of Li-bearing batteries, which will have at first to be produced. Hence lithium mining is and will be promoted as well as the research for the best beneficiation process (Tadesse et al., 2019; Yelatontsev and Mukhachev, 2021), justifying the need for fast and accurate analysis of Li ores.

In order for lithium to be analysed in minerals, specific techniques have to be used such as laser ablation ICP-MS (Breiter et al., 2017), Li content recalculation on the basis of quantitative powder XRD (Pöllmann and König, 2021), wet chemical analysis (Černy et al., 1997), soft X-ray emission spectroscopy (SXES, MacRae et al., 2018; Terauchi et al., 2014; Yamamoto et al., 2020), SIMS (Marschall and Tang, 2020), ToF-SIMS (Aylmore et al., 2018). Wavelength dispersive spectroscopy (WDS, or electron microprobe) has been used to assess indirectly the presence of Li (Tischendorf et al., 1997; Tischendorf et al., 1999; Yavuz, 2001) but some recent works have been successful to detect it in alloys (Robbes et al., 2017), despite the difficulty to measure low-energy X-

rays (Llovet et al., 2021; Polkonikov et al., 2021; Schweizer et al., 2022).

It can hence be seen that there are analytical solutions for Li in minerals. However, it is of interest to investigate further possibilities. Indeed, since its inception >50 years ago (Keil et al., 2009), energy dispersive spectroscopy (EDS) and the use of solid-state detectors (Fitzgerald et al., 1968) has tremendously contributed to the broad field of materials characterization. Recent developments in windowless energy dispersive spectroscopy already allow to detect and (semi) quantify the presence of lithium (Hovington et al., 2016; Xiaobing et al., 2013; Yamamoto et al., 2016). With the ever-increasing demand of this element, fast, accurate and reliable data will have to be obtained.

Moreover, the chemical environment of Li influences its EDS analysis (Hovington et al., 2016). Namely, it has been shown, on the basis of Monte Carlo simulation of Li emitted X-ray intensity, that depending on the type of compound, the correlation between Li K intensity do not always correlate with Li content. In a TEM-based EDS study of LiCl, Gauvin et al. (2021) have observed the volatilization of Cl and the transformation of this compound into metallic Li, resulting in a strong evolution of the Li K α peak intensity with time.

The present paper proposes to simulate the EDS spectra of the main

* Corresponding author at: IMT Nord Europe, Institut Mines-Télécom, Centre for Materials and Processes, F-59000 Lille, France.

E-mail address: vincent.thiery@imt-nord-europe.fr (V. Thiery).

Table 1

Typical Li-bearing ore minerals, arranged by alphabetical order, with structural formula, density, mean atomic number and calculated backscattered coefficient. Quartz and albite are not Li-bearing minerals, but since they are likely to form their gangue they can be used as reference for comparison.¹ for Mg:Li = 1:1² for OH:F = 1:1. Atomic weights based on 2019 IUPAC data (<https://iupac.qmul.ac.uk/AtWt/>).

Phase	Composition	LiO ₂ wt%	Li mass fraction	Density	\bar{Z}	η
Amblygonite	LiAl(PO ₄)F	7.4	3.44	3.04–3.11	10.27	0.1202
Bikitaite	LiAlSi ₂ O ₆ H ₂ O	7.32	3.40	2.29–2.30	9.84	0.1148
Eucryptite	LiAlSiO ₄	9.7	4.51	2.65–2.66	10.13	0.1185
Hectorite ¹	Na _{0.3} (Mg,Li) ₃ (Si ₄ O ₁₀)(F,OH) ₂	<1–3	0.46–1.39	2.3	10.21	0.1195
Jadarite	LiNaSi ₂ O ₅ (OH)	7.3	3.39	2.45	8.45	0.0970
Lepidolite series	Polylithionite	KLi ₂ Al(Si ₄ O ₁₀)(F,OH) ₂	4.19	1.95	2.58–2.82	11.04
	Trilithionite	K(Li _{1.5} Al _{1.5})(AlSi ₃ O ₁₀)(F,OH) ₂			2.8–2.9	11.10
Montebrasite ²	LiAl(PO ₄)(OH, F)	7.4	3.44	2.98–3.04	10.20	0.1193
Petalite	LiAlSi ₄ O ₁₀	4.73	2.20	2.412–2.422	10.53	0.1234
Spodumene	LiAlSi ₂ O ₆	6–9	2.79–4.18	3.03–3.23	9.50	0.1105
Triphylite	Li(Fe,Mn)PO ₄	9.47	4.4	3.50–3.58	15.32	0.1791
Zinnwaldite	Polylithionite	See above		See above	See above	See above
	Siderophyllite	KFe ₂ ⁺ Al(Al ₂ Si ₂ O ₁₀)(OH) ₂	2–5	0.93–2.32	Not of interest	Not of interest
Quartz	SiO ₂	n/a			10.80	0.1268
Orthoclase	KAlSi ₃ O ₈	n/a			11.85	0.1394

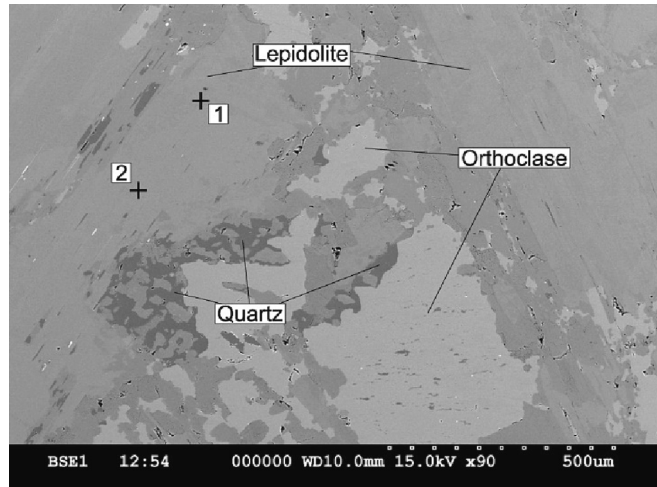


Fig. 1. BSE image (polished cross-section) of a lepidolite-bearing granite. Lepidolite is characterized by its elongated cleavage. Theoretical backscattered coefficients (Table 1) are in good agreement with the grey levels of the different phases. Spectrum for point 1 is shown in Fig. 2, for point 2 in Fig. 3.

Li-bearing minerals, i.e. the ones of economic interest. Hence, microscopists which will carry out further work based on EDS measurements with windowless detectors will be likely to have an idea of what to expect. In order to make a comparison between simulation and actual results, some EDS spots obtained using a classical (i.e. with a window) SDD detector on two Li-bearing minerals (lepidolite and spodumene, Table 1) are presented. The investigated minerals have a much more complex chemistry than previously studied binary Li compounds or pure Li EDS analysis (Hovington et al., 2016; Xiaobing et al., 2013).

Also, since minerals occur altogether (the so-called “rock-forming minerals”), backscattering coefficients for the main Li ore minerals are calculated. Hence, an evaluation of the contrasts likely to be present in backscattering mode under the SEM is possible. It can be used in order to relate a backscattered electrons (BSE) intensity to a chemical information (Čalkovský et al., 2023). In the present case, a lepidolite-bearing granite is studied in order to illustrate BSE contrasts.

1.1. Challenges in Li analysis by the means of energy dispersive spectroscopy

Those challenges have already been extensively discussed and reviewed by Hovington et al. (2016) but will be briefly reminded here.

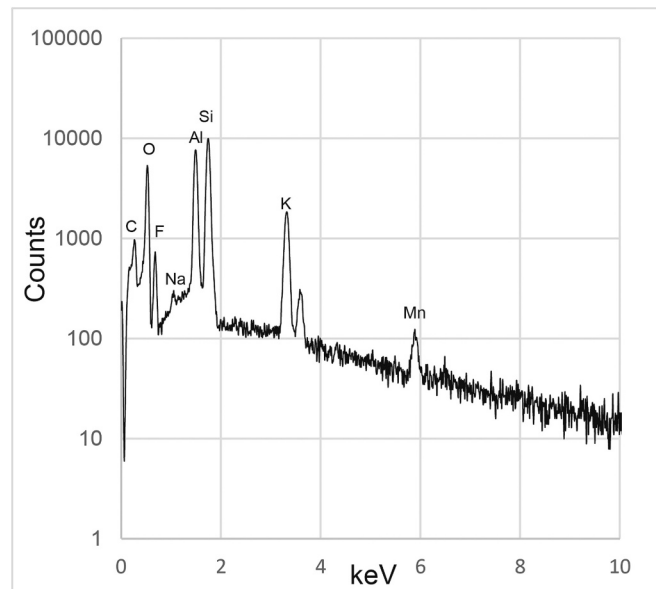


Fig. 2. EDS spectrum of lepidolite obtained at 15 kV (point 1 on Fig. 1) using an EDS detector equipped with a Norvar window.

Lithium, with an atomic number of 3 and a density of 0.54 g.cm⁻³ is a light element. Its characteristic X-ray emission belongs to the so-called “soft X-rays”, even “ultra-soft X-rays”. Indeed, its characteristic K α line, initially measured at 43.07 eV (Rollefson, 1925) is now recognized at 54.3 eV (X-ray data booklet, Center for X-ray Optics and Advanced Light Source, Lawrence Berkeley National Laboratory). Databases for X-ray energies also include the seminal work of Cauchois and Sénemaud (1978) recently brought up to date by Jonnard and Bonnelle (2011); the synthesis from Zschornack (2007) is also worth mentioning.

In a classical EDS detector of SDD type, such X-rays are stopped by the window and do not reach the detector. Hence, the new generation of windowless detectors allow to analyse Li (Burgess et al., 2013; Hovington et al., 2016; Xiaobing et al., 2013), but face the challenges of low beam energy analysis (Bloomfield et al., 1984; Newbury and Ritchie, 2016; Hovington et al., 2016).

The choice of ideal analytical conditions, i.e. the accelerating voltage allowing a good deadtime (Newbury and Ritchie, 2013), is already sometimes tricky in non Li-bearing materials in order to avoid sum peaks for example. In Li-bearing compounds, and to a broader extent in light elements-bearing compounds, X-ray intensities of light elements

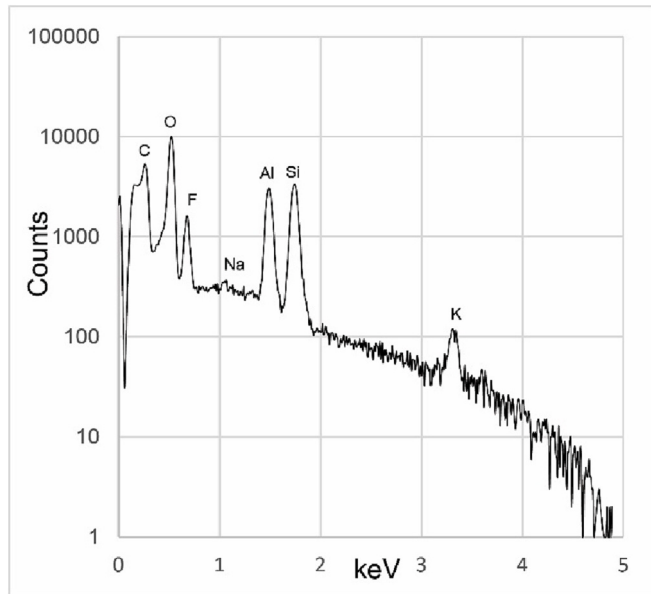


Fig. 3. EDS spectrum of lepidolite obtained at 5 kV (point 2 on Fig. 1) using an EDS detector equipped with a Norvar window.

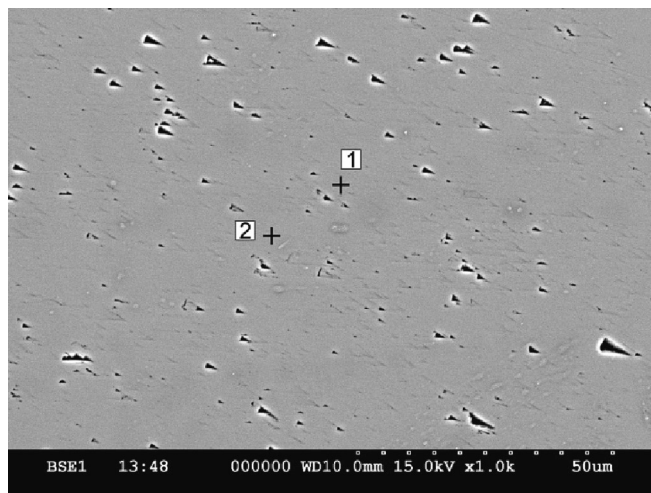


Fig. 4. BSE image (polished cross-section) of spodumene. Spectrum for point 1 is shown in Fig. 5, for point 2 in Fig. 6.

characteristics lines can be increased by working with low accelerating voltages around 5 kV (Schweizer et al., 2022). Depending on the mass absorption coefficient, Hovington et al. (2016) have proposed to work up to 5 kV for materials which do not absorb Li in excess down to 2 kV for materials in which absorption is higher.

1.2. SEM-BSE

1.2.1. Generation of contrast

Phase contrast in backscattered electrons mode under the scanning electron microscope depends on the atomic number of the elements present in the analysed phase (Joy, 1991). The heavier the element, the lighter the grey level on the micrograph, and contrarily for light elements. For minerals, a factor known as average (or mean) atomic number, \bar{Z} , has to be calculated or estimated from micrographs (Sánchez et al., 2012). It is assumed to be the sum of the mass fractions of the atomic numbers in the composition and is expressed this way (Donovan et al., 2019):

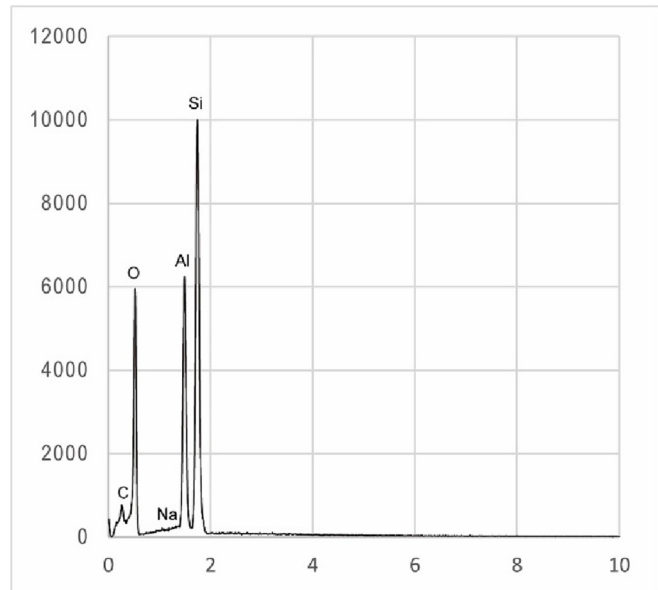


Fig. 5. EDS spectrum of spodumene obtained at 15 kV (point 1 on Fig. 4).

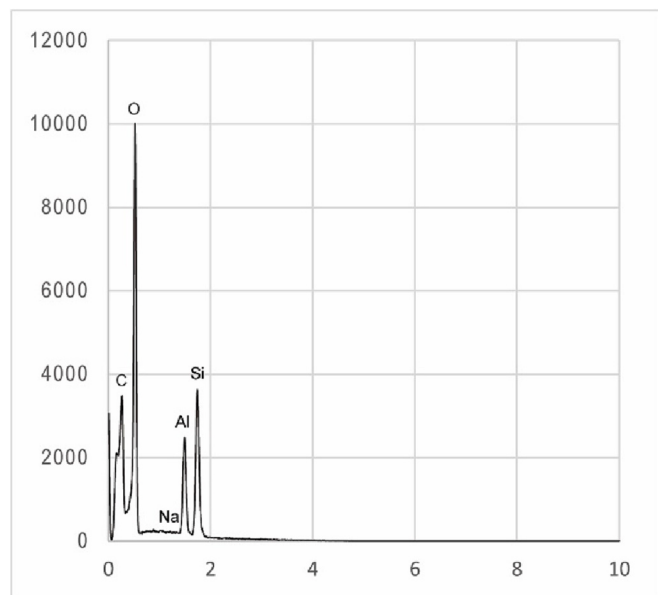


Fig. 6. EDS spectrum of spodumene obtained at 5 kV (point 2 on Fig. 4).

$$\bar{Z}_{(c_i)} = \sum_{i=1}^n c_i Z_i$$

Z_i represents the atomic number of the element i , c_i stands for the mass fraction of element i . From this factor, the backscattering coefficient η can be calculated as follows (Reimer, 1998):

$$\eta = -0.0254 + 0.016Z - 1.86 \times 10^{-4}Z^2 + 8.3 \times 10^{-7}Z^3$$

1.2.2. Li-bearing minerals and their backscattering coefficient

In January 2023, the International Mineralogical Association (IMA) recognizes 121 mineral species which contains lithium (see also Grew, 2020). Only a minority of them are exploited as ores, they are listed in Table 1 (see also Bowell et al., 2020). It can be noted that one lithium-bearing mineral, namely spodumene LiAl_2O_6 , belonging to the pyroxene group (Morimoto, 1988) is also used in gemmology and known as kunzite when it is pink or hiddenite when green.

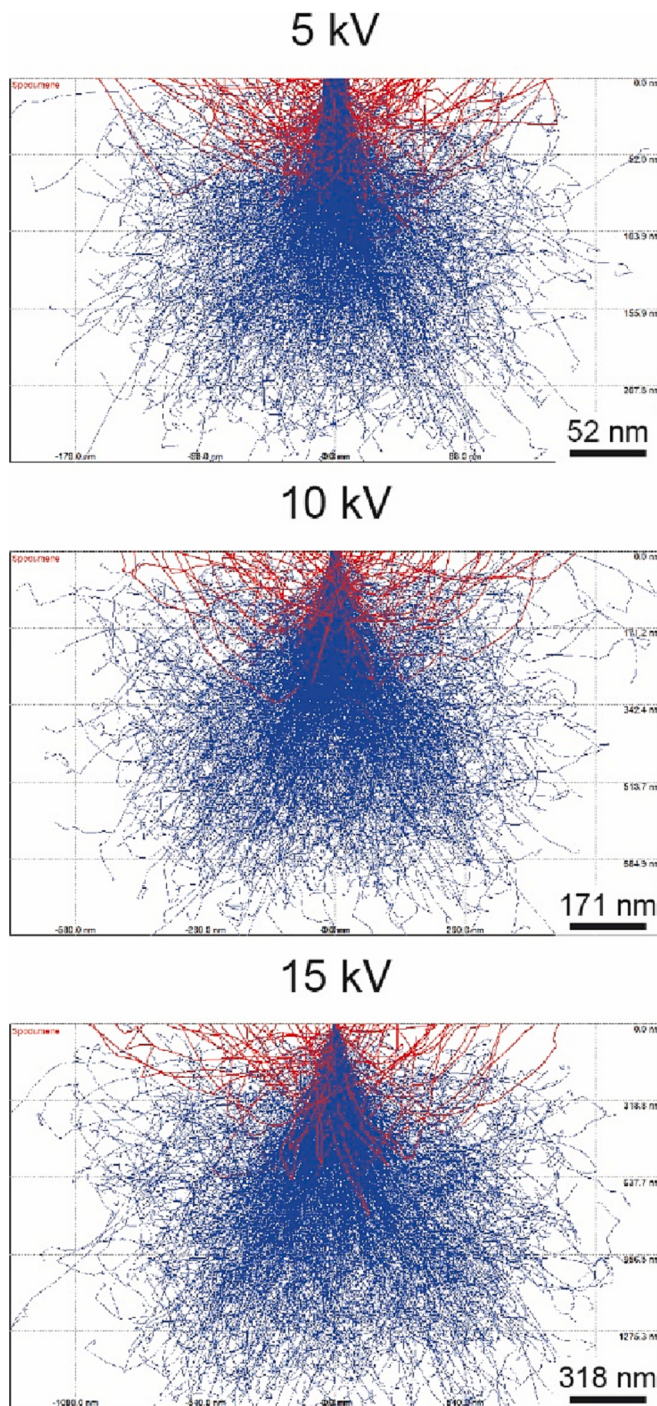


Fig. 7. Monte Carlo simulation of electron-matter interactions in spodumene at 5, 10 and 15 keV. Blue trajectories correspond to absorbed electrons, red ones to backscattered electrons. Simulations for common ore Li-bearing minerals of Table 1 are given in supplementary materials. (For interpretation of the references to colour in this figure legend, the reader is referred to the web version of this article.)

Minerals of interest in lithium mining are mostly silicates, such as petalite, spodumene or lepidolite, exploited in pegmatites (Beskin and Marin, 2018; Simmons et al., 2019; Yelatontsev and Mukhachev, 2021). Lepidolite is actually not a mineral species as such but it describes a series of micas which compositions lie within the poly lithionite-trilithionite series (Table 1). In the same way, zinnwaldite is not a mineral species but it refers to the compositional span between poly lithionite and siderophyllite (Table 1). This is a classic ore in lithium

Table 2

X-ray attenuation lengths at 54 eV for Li-bearing minerals (see Table 1) calculated using https://henke.lbl.gov/optical_constants/atten2.html (accessed 04/27/2023).

Phase	Attenuation length in nm
Amblygonite	17
Bikitaita	26
Eucryptite	24
Hectorite ¹	21
Jadarite	18
Lepidolite series	Poly lithionite Trilithionite
Montebrasite ²	21 20
Petalite	17 24
Spodumene	19
Triphyllite	16

mining (Schneider et al., 2017). Phosphates (amblygonite, montebrasite) also play an important role. The recently discovered jadarite (Stanley et al., 2007) is a borosilicate.

Not of interest as an ore, but rather as a mineral curiosity, the fluoride griceite LiF (Van Velthuizen and Chao, 1989) is the natural analogue of the LiF compound used in batteries (Ko and Yoon, 2019).

It can be thus seen that natural occurrences of lithium concern a broad range of chemical environments for this element (other Li-bearing minerals, which are not of economic interest and hence not discussed here, are really varied in terms of composition, such as for example lithiowodginite LiTa₃O₈ or sogdianite KZr₂Li₃Si₁₂O₃₀).

2. Materials and methods

The present study is mostly based on the simulation of microanalysis, however, some actual samples of Li-bearing minerals have been studied under the SEM in order to provide a comparison.

Lepidolite (Atelier la trouvaille, France) and spodumene (Le comptoir géologique, France) have been prepared according to classic polishing methods (Humphries, 1992) down to one micrometer diamond paste.

Scanning electron microscopy has been carried out on a Hitachi S-4300SE/N SEM (Hitachi High-Technologies corporation) working in high vacuum mode, coupled to a Thermoscientific Ultradry EDX detector (Thermo Fischer Scientific Inc.). More specifically, the detector is a SDD type, with a Norvar window of a thickness of 0.43 μm. The take-off angle is 30°. All spectra presented in Figs. 2, 3, 5 and 6 have a C peak due to the carbon coating of the polished sample.

Monte Carlo simulation of electron-matter interactions was done using Casino V2.51 (Drouin et al., 2007). It provides an insight of the size and shape of interaction volume as well as the distribution of the backscattered electrons providing important information for image interpretation in SEM.

Finally, the EDS spectra simulation was done using NIST-DTSA II Microscopium software (Newbury and Ritchie, 2015; Ritchie et al., 2012). In order to mimic the latest developments in windowless detectors, parameters similar to the Oxford Ultim® Extreme detector have been introduced. Namely, the surface of the detector has been set to 100 mm².

3. Results

3.1. BSE microstructure and EDS spectra

3.1.1. Lepidolite

The sample consists mainly of lepidolite, quartz and orthoclase, yielding three different backscattering coefficients (Table 1). Quartz, with the lower one, has the darkest hue on a BSE micrograph (Fig. 1) whereas orthoclase has the highest and appears thus as the brightest rock-forming phase (small dots bright dots might be iron oxides

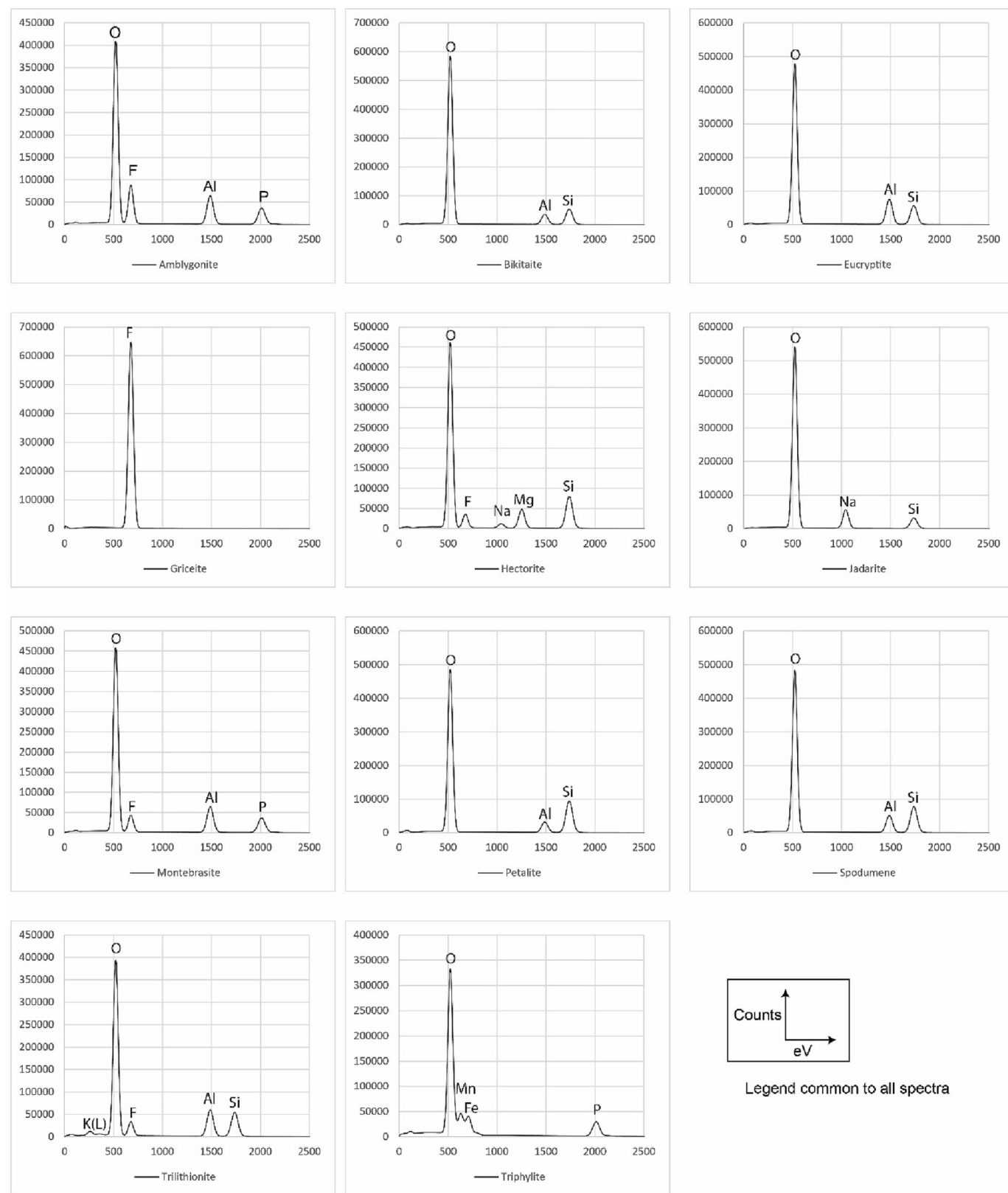


Fig. 8. Simulated EDS spectra at 5 keV for the common Li-bearing ore minerals.

inclusions). Lepidolite lies between and can furthermore be identified thanks to its cleavage.

The EDS spectrum obtained at 15 kV (Fig. 2) depicts all expected elements, save for Li which could not be measured on a SDD with window detector. The presence of Na and Mn as minor impurities is not

surprising since the range of chemical elements which can be incorporated in micas is wide (Rieder et al., 1998).

At 5 kV (Fig. 3), the Mn-K α line (5.89 keV) is not excited. However, all other elements (with the exception of Li for the aforementioned analytical reason) are clearly distinguishable.

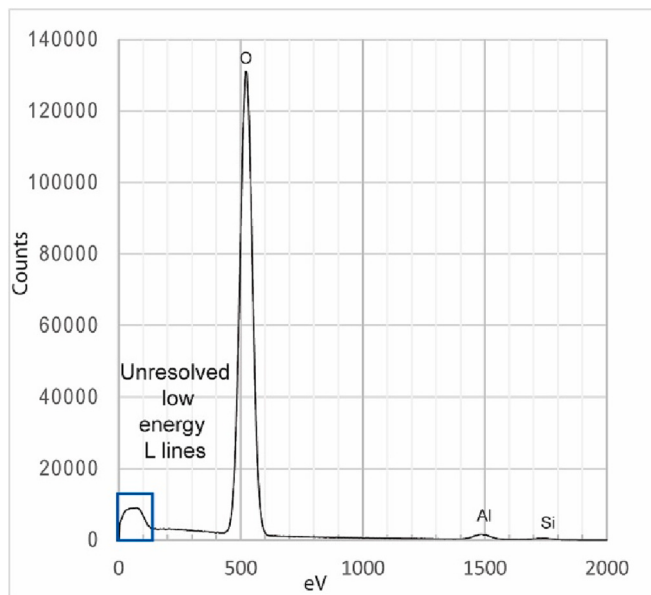


Fig. 9. Simulation of an EDS spectrum of spodumene at 2 keV using DTSA II Microscopium software.

3.1.2. Spodumene

The *gem* spodumene investigated here is pure hence it does not display any change of grey level in BSE; its only feature is its cleavage appearing as regular triangular pits all over the surface (Fig. 4).

The EDS spectrum at 15 kV (Fig. 5), exception of Li, shows a very pure spodumene ($\text{LiAlSi}_2\text{O}_6$), the slight content in Na is not surprising for a pyroxene (Morimoto, 1988). At 5 kV (Fig. 6) there is no significant difference.

3.1.3. Monte Carlo simulation of electron-matter interactions

The visual representation of the Monte Carlo simulation of the electron-matter interaction zone is of interest in the case of the study of microstructures in which crystal sizes are small. Indeed, it can guide the operator towards a better understanding of what is really analysed, and the limitations in the cases of overlaps when two phases are analysed simultaneously. The simulation results (Fig. 7 and supplementary materials) shows that the interaction volume increases with the accelerating voltage for all the listed minerals. Minerals having higher average atomic number have more backscattered electrons, for example jadarite with the lowest average atomic number has lesser backscattered electrons in comparison with amblygonite at the same accelerating voltage 5 kV. This is in good agreement with the calculated backscattered coefficient shown in Table 1.

For the phosphates, typically montebrasite and amblygonite, simulation results show that the interaction volume can go from an average diameter of 171 nm at 5 keV, to 560 nm at 10 keV and to 1158 nm at 20 keV. For jadarite which is a borosilicate, the interaction volume spans from a diameter of 184 nm at 5 keV, to 800 nm at 10 keV and to 1420 nm at 15 keV. Consequently, the interaction volume is deeper for borosilicates in comparison with phosphates. However, it is not the same case with silicates: they do not show a close range of interaction depth values with increasing voltage. A significant difference is noted for instance: trilithionite's interaction depth, with a diameter of ca. 2600 nm at 15 keV is way bigger than the spodumene's one at the same voltage (ca. 1080 nm).

3.1.4. X-ray attenuation

Within materials, the decrease of X-rays intensity is expressed as:

$$I = I_0 e^{-\mu x}$$

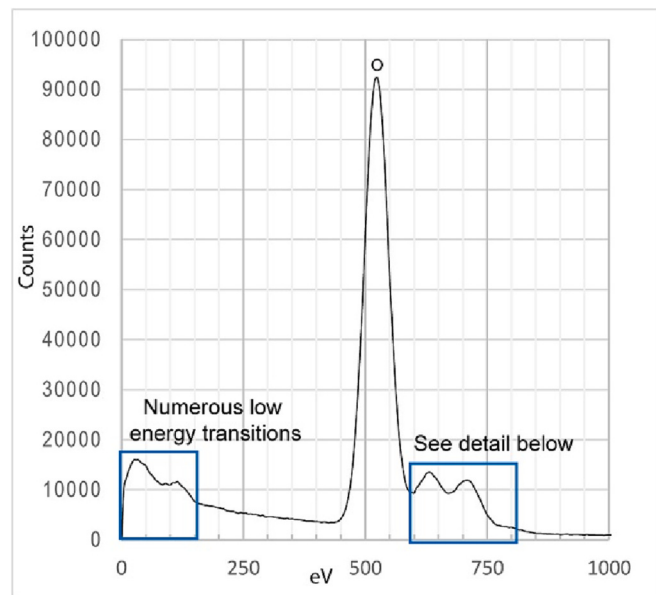


Fig. 10. Simulation of an EDS spectrum at 2 keV for triphyllite (top) and close-up view of the theoretical Mn and Fe La lines compared to the computed spectrum.

I_0 refers to the initial intensity, I to the intensity after a path x and μ the linear attenuation coefficient. The attenuation length is defined as the depth into the material measured along the surface normal where the intensity of x-rays falls to $1/e$ of its value at the surface. Table 2 presents attenuation length for minerals detailed in Table 1. They all fall within the 16–24 nm range, there does not seem to be any evident correlation with mineral chemistry.

This very narrow range of attenuation lengths has to be compared with Monte Carlo simulations of electron-matter interactions (Fig. 7). Indeed, while the depth of penetration of electron exceeds 200 nm at 5 kV, the X-ray attenuation for the Li characteristic line will be quickly attenuated in the sample.

3.1.5. EDS spectra simulation

EDS spectra provide a good, easy to use visual tool to identify minerals (Severin, 2005). However, in the very specific case of Li-bearing minerals, and in the present state-of-the art of available detectors, the

detection of Li is still a challenge (see above). Hence, despite parameters promoting the detection of Li (see the materials & methods section), simulated spectra only display elements after C. Simulated spectra of the main ore, Li-bearing minerals, as well as griceite LiF, are presented in Fig. 8. Low energy lines, in the 40–100 eV range, are not resolved and generate a small bump in the spectra. The resolution provided by the software is 132 eV, corresponding to the full width at mid height of the Mn K α line (5.89 keV); the resolution for energies lower than 100 eV being of 40–50 eV at best (Brodusch et al., 2020).

4. Discussion, perspectives and conclusions

Lithium mineralogy is a specific branch in geosciences, so is it regarding its microanalysis (Hovington et al., 2016; Xiaobing et al., 2013). Researchers dealing with Li-bearing minerals are already used to state-of-the-art techniques to characterize them.

Li-bearing minerals containing elements which have peaks above 5 kV will be difficult to analyse correctly. For example, in the case of lepidolite, the Mn content might be totally missed if the analysis is carried out at 5 kV only (Fig. 3). Silicates such as spodumene (Fig. 6) are not problematic since Si and Al K peaks are under 2 kV.

The Monte Carlo simulation is a good tool to provide information about X-rays depth: it is useful to simulate the electron sample interaction based on the material chemical composition and the accelerated voltages at once. In this paper, all the Li-bearing minerals show a complex chemical composition (Table 1). However, regarding their chemistry, the challenge of low voltage analysis lies in the fact that for most of them the emission lines are not excited. For example, in the case of spodumene, the K α lines of Al (1,48 keV) and Si (1,73 keV), although weak, can be observed on a simulation at 2 keV (Fig. 9): all the qualitative chemical information is present. However, low energy L-lines are not resolved, resulting in a bump centred around 50 eV – the Li K α line is located at 54.3 eV; Si and Al have several L lines below 155 eV which cannot be resolved by EDS (Zschornack, 2007).

For minerals containing elements with higher Z, the use of the L lines is useful but difficult to implement for energies lower than 200 eV. For example, in the case of triphyllite (Fig. 10), L α and L β for Mn and Fe are 637,4 and 705 eV, respectively. However, for P, all K lines are above 2 keV. For this element also, L lines fall within the ca. 48–189 eV (Zschornack, 2007), making their detection difficult (if not impossible) for the same reasons as discussed above for Li.

It is of importance to highlight that Mg L and Al L lines are close to the Li K α line, several lines being around 49 eV for Mg and 69 eV for Al. Hence, in the aforementioned Li-bearing minerals of economic importance (Table 1) which contain Mg and/or Al, the presence of poorly resolved low energy peaks are likely to complicate the correct identification of the Li line as shown in Fig. 9. For other Li-bearing minerals, which are not common, such as for example simferite LiMg(PO₄) (Bayrakov et al., 2005), the use of the L lines with a low accelerating voltage might be problematic. Also, Li-bearing amphiboles, which are defined as amphiboles containing up to three Li atom per formula unit (Oberti et al., 2003), all contain Al and/or Mg. This Li content being, for example, up to 3.98% Li₂O in ferripedrizite (Caballero et al., 2002), it opens the way to interesting geomaterials to analyse with EDS.

To broaden the discussion, it must be noted that lepidolite has some prospects for use in Li–S batteries (Zeng et al., 2021). Hence, the challenges of SEM-EDS analyses of Li in minerals are likely to open towards this domain with compounds relatively close to natural ones. Indeed, the aforementioned triphyllite has the same chemistry as the famous lithium-iron-phosphate (LFP) cathodes used in batteries.

To conclude, it is important to note that the present study documents minerals which are likely to be less beam-sensitive than previously reported Li-bearing compounds (or pure elemental Li) which are likely to be damaged or to display chemical changes during the analysis (Gauvin et al., 2021; Hovington et al., 2016; Xiaobing et al., 2013). Indeed, the weathering of spodumene into smectite (Singh and Gilkes, 1993) is very

unlikely to take place under the SEM, and lepidolite has been shown to be a very stable mica (Leonard and Weed, 1970).

Finally, either using WDS or EDS, the short attenuation lengths of the characteristic X-ray line of Li (Table 2) will account for difficulties in its quantification in minerals. However, a careful investigation based on adequate analytical conditions can confidently lead to its identification.

Supplementary data to this article can be found online at <https://doi.org/10.1016/j.chemgeo.2023.121573>.

Declaration of Competing Interest

The authors declare that they have no known competing financial interests or personal relationships that could have appeared to influence the work reported in this paper.

Data availability

Data will be made available on request.

References

- Aylmore, M.G., Merigot, K., Quadir, Z., Rickard, W.D.A., Evans, N.J., McDonald, B.J., Catovic, E., Spitalny, P., 2018. Applications of advanced analytical and mass spectrometry techniques to the characterisation of micaceous lithium-bearing ores. Miner. Eng. 116, 182–195. <https://doi.org/10.1016/j.mineng.2017.08.004>.
- Bayrakov, V., Yakubovich, O., Simonov, A., Borisovskiy, S.E., Ziborova, T.A., 2005. Simferite Li(Mg,Fe₃₊,Mn₃₊)₂[PO₄]₂ - a new mineral. Mineralogiceskij Zhurnal 27, 112–120.
- Beskin, S.M., Marin, Yu.B., 2018. Classification of granitic pegmatites and pegmatite-bearing granitic systems. Geol. Ore Deposits 60, 578–586. <https://doi.org/10.1134/S1075701518070024>.
- Bibienne, T., Magnan, J.-F., Rupp, A., Laroche, N., 2020. From Mine to mind and Mobiles: Society's increasing Dependence on Lithium. Elements 16, 265–270. <https://doi.org/10.2138/gselements.16.4.265>.
- Bloomfield, D.J., Love, G., Scott, V.D., 1984. Quantitative light element analysis using an energy dispersive detector. 1-D dead time and the low-energy spectrum. X-Ray Spectrom. 13, 69–77. <https://doi.org/10.1002/xrs.1300130207>.
- Bowell, R.J., Lagos, L., de los Hoyos, C.R., Declercq, J., 2020. Classification and Characteristics of Natural Lithium Resources. Elements 16, 259–264. <https://doi.org/10.2138/gselements.16.4.259>.
- Breiter, K., Vaňková, M., Galiová, M.V., Korbelová, Z., Kanický, V., 2017. Lithium and trace-element concentrations in trioctahedral micas from granites of different geochemical types measured via laser ablation ICP-MS. Mineral. Mag. 81, 15–33. <https://doi.org/10.1111/minmag.2016.080.137>.
- Brodusch, N., Zaghib, K., Gauvin, R., 2020. Improvement of the energy resolution of energy dispersive spectrometers (EDS) using Richardson–Lucy deconvolution. Ultramicroscopy 209, 112886. <https://doi.org/10.1016/j.ultramic.2019.112886>.
- Burgess, S., Li, X., Holland, J., 2013. High spatial resolution energy dispersive X-ray spectrometry in the SEM and the detection of light elements including lithium. Microscopy A 27, S8–S13.
- Caballero, J.M., Oberti, R., Ottolini, L., 2002. Ferripedrizite, a new monoclinic BLi amphibole end-member from the Eastern Pedriza Massif, Sierra de Guadarrama, Spain, and a restatement of the nomenclature of Mg–Fe–Mn–Li amphiboles. Am. Mineral. 87, 976–982. <https://doi.org/10.2138/am-2002-0721>.
- Čalkovský, M., Müller, E., Gerthsen, D., 2023. Quantitative analysis of backscattered-electron contrast in scanning electron microscopy. J. Microsc. 289, 32–47. <https://doi.org/10.1111/jmi.13148>.
- Cauchois, Y., Sénémaud, C., 1978. Tables of Wavelengths of X-Ray Emission Lines and Absorption Edges (International Tables of Selected Constants 18). Pergamon Press, Oxford.
- Cerny, P., Chapman, R., Schreyer, W., Ottolini, L., Bottazzi, P., McCammon, C.A., 1997. Lithium in sekaninaite from the type locality, Dolni Bory, Czech Republic. Can. Mineral. 35, 167–173.
- Donovan, J., Fellowes, J., McMorran, B., 2019. Average Atomic Number and Electron Backscattering in Compounds. Microsc. Microanal. 25, 2314–2315. <https://doi.org/10.1017/S1431927619012303>.
- Drouin, D., Réal Couture, A., Joly, D., Tastet, X., Aimez, V., Gauvin, R., 2007. CASINO V2.42—a fast and easy-to-use modeling tool for scanning electron microscopy and microanalysis users. Scanning 29, 92–101.
- Fitzgerald, R., Keil, K., Heinrich, K.F.J., 1968. Solid-State Energy-Dispersion Spectrometer for Electron-Microprobe X-ray Analysis. Science 159, 528–530. <https://doi.org/10.1126/science.159.3814.528>.
- Gauvin, R., Brodusch, N., Voisard, F., Dumaresq, N., Zaghib, K., Demers, H., Trudeau, M., 2021. EDS of Lithium Materials from 0.5 to 30 keV. Microsc. Microanal. 27, 1868–1869. <https://doi.org/10.1017/S1431927621006814>.
- Grew, E.S., 2020. The Minerals of Lithium. Elements 16, 235–240. <https://doi.org/10.2138/gselements.16.4.235>.
- Hovington, P., Timoshivskii, V., Burgess, S., Demers, H., Statham, P., Gauvin, R., Zaghib, K., 2016. Can we detect Li K X-ray in lithium compounds using energy

- dispersive spectroscopy? Scanning 38, 571–578. <https://doi.org/10.1002/sca.21302>.
- Humphries, D.W., 1992. The Preparation of Thin Sections of Rocks, Minerals, and Ceramics. Oxford University Press.
- Jonnard, P., Bonnelle, C., 2011. Cauchois & Sénemaud Tables of wavelengths of x-ray emission lines and absorption edges, P. Jonnard and C. Bonnelle, X-Ray Spectrom. 40, 12–16. X-Ray Spectrom. 40, 12–16.
- Joy, D.C., 1991. Contrast in high-resolution scanning electron microscope images. J. Microsc. 161, 343–355. <https://doi.org/10.1111/j.1365-2818.1991.tb03095.x>.
- Keil, K., Fitzgerald, R., Heinrich, K.F.J., 2009. Celebrating 40 years of Energy Dispersive X-Ray Spectrometry in Electron Probe Microanalysis: a Historic and Nostalgic look Back from the Beginnings. Microsc. Microanal. 15, 476–483. <https://doi.org/10.1017/S1431927609990377>.
- Ko, J., Yoon, Y.S., 2019. Recent progress in LiF materials for safe lithium metal anode of rechargeable batteries: is LiF the key to commercializing Li metal batteries? Ceram. Int. 45, 30–49. <https://doi.org/10.1016/j.ceramint.2018.09.287>.
- Leonard, R.A., Weed, S.B., 1970. Mica Weathering rates as Related to Mica Type and Composition. Clay Clay Miner. 18, 187–195. <https://doi.org/10.1346/CCMN.1970.0180402>.
- Lovett, X., Moy, A., Pinard, P.T., Fournelle, J.H., 2021. Electron probe microanalysis: a review of recent developments and applications in materials science and engineering. Prog. Mater. Sci. 116, 100673 <https://doi.org/10.1016/j.pmatsci.2020.100673>.
- MacRae, C.M., Hughes, A.E., Laird, J.S., Glenn, A.M., Wilson, N.C., Torpy, A., Gibson, M.A., Zhou, X., Birbilis, N., Thompson, G.E., 2018. An Examination of the Composition and Microstructure of Coarse Intermetallic Particles in AA2099-T8, including Li Detection. Microsc. Microanal. 24, 325–341. <https://doi.org/10.1017/S1431927618000454>.
- Marschall, H.R., Tang, M., 2020. High-Temperature Processes: is it Time for Lithium Isotopes? Elements 16, 247–252. <https://doi.org/10.2138/gselements.16.4.247>.
- Morimoto, N., 1988. Nomenclature of pyroxenes. Bull. Mineral. 535–550.
- Newbury, D.E., Ritchie, N.W.M., 2013. Is Scanning Electron Microscopy/Energy Dispersive X-ray Spectrometry (SEM/EDS) Quantitative? Scanning 35, 141–168. <https://doi.org/10.1002/sea.21041>.
- Newbury, D.E., Ritchie, D.W.M., 2015. Performing elemental microanalysis with high accuracy and high precision by scanning electron microscopy/silicon drift detector energy-dispersive X-ray spectrometry (SEM/SDD-EDS). J. Mater. Sci. 50, 493–518.
- Newbury, D.E., Ritchie, N.W.M., 2016. Electron-Excited X-Ray Microanalysis at Low Beam Energy: almost always an Adventure! Microsc. Microanal. 22, 735–753. <https://doi.org/10.1017/S1431927616011521>.
- Oberti, R., Cámará, F., Ottolini, L., Caballero, J.M., 2003. Lithium in amphiboles: detection, quantification, and incorporation mechanisms in the compositional space bridging sodic and BLi-amphiboles. Eur. J. Mineral. 15, 309–319. <https://doi.org/10.1127/0935-1221/2003/0015-0309>.
- Polkonikov, V., Chkhalo, N., Pleshkov, R., Giglia, A., Rividi, N., Brackx, E., Le Guen, K., Ismail, I., Jonnard, P., 2021. Periodic Multilayer for X-ray Spectroscopy in the Li K Range. Appl. Sci. <https://doi.org/10.3390/app11146385>.
- Pöllmann, H., König, U., 2021. Monitoring of Lithium Contents in Lithium Ores and Concentrate-Assessment using X-ray Diffraction (XRD). Minerals 11, 1058.
- Reimer, L., 1998. Scanning Electron Microscopy - Physics of Image Formation and Microanalysis. Springer.
- Rieder, M., Cavazzini, G., D'Yakonov, Y.S., Frank-Kamenetskii, V.A., Gottardi, G., Guggenheim, S., Koval, P.V., Mueller, G., Neiva, A.M.R., Radoslovich, E.W., Robert, J.-L., Sassi, F.P., Takeda, H., Weiss, Z., Wones, D.R., 1998. Nomenclature of the micas. Can. Mineral. 36, 905–912.
- Ritchie, N.W.M., Newbury, D.E., Davis, J.M., 2012. EDS Measurements of X-Ray Intensity at WDS Precision and Accuracy using a Silicon Drift Detector. Microsc. Microanal. 18, 892–904. <https://doi.org/10.1017/S1431927612001109>.
- Robbes, A., Henderson, C., Moret, M., Kelly, T., Larson, D., 2017. Lithium detection by wavelength-dispersive X-ray spectrometry in an electron probe microanalyzer (EPMA). In: Goldsmith Abstracts, p. 3367.
- Rollefson, G.K., 1925. Characteristic X-Rays from lithium. Phys. Rev. 25, 740–746. <https://doi.org/10.1103/PhysRev.25.740>.
- Sánchez, E., Deluigi, M.T., Castellano, G., 2012. Mean Atomic Number Quantitative Assessment in Backscattered Electron Imaging. Microsc. Microanal. 18, 1355–1361. <https://doi.org/10.1017/S1431927612013566>.
- Schneider, A., Schmidt, H., Meven, M., Brendler, E., Kirchner, J., Martin, G., Bertau, M., Voigt, W., 2017. Lithium extraction from the mineral zinnwaldite: part I: effect of thermal treatment on properties and structure of zinnwaldite. Miner. Eng. 111, 55–67. <https://doi.org/10.1016/j.mineng.2017.05.006>.
- Schweizer, P., Brackx, E., Jonnard, P., 2022. Electron probe microanalysis of light elements: Improvements in the measurement and signal extraction methods. X-Ray Spectrom. 51, 403–412. <https://doi.org/10.1002/xrs.3290>.
- Severin, K.P., 2005. Energy Dispersive Spectrometry of Common Rock Forming Minerals. Springer.
- Simmons, W.B., Falster, A.U., Nizamoff, J.W., Freeman, G., 2019. Giant spodumene and montebrasite crystals from the Plumbago North pegmatite, Oxford County, Maine. Can. Mineral. 57, 795–797. <https://doi.org/10.3749/canmin.AB00024>.
- Singh, B., Gilkes, R.J., 1993. Weathering of Spodumene to Smectite in a Lateritic Environment. Clay Clay Miner. 41, 624–630. <https://doi.org/10.1346/CCMN.1993.0410513>.
- Stanley, C.J., Jones, G.C., Rumsey, M.S., Blake, C., Roberts, A.C., Stirling, J.A.R., Carpenter, G.J.C., Whitfield, P.S., Grice, J.D., Lepage, Y., 2007. Jadarite, Li₂Na₂B₃O₇(OH), a new mineral species from the Jadar Basin, Serbia. Eur. J. Min. Eur. J. Mineral. 19, 575–580.
- Tadesse, B., Makuei, F., Albijanic, B., Dyer, L., 2019. The beneficiation of lithium minerals from hard rock ores: a review. Miner. Eng. 131, 170–184. <https://doi.org/10.1016/j.jmineng.2018.11.023>.
- Terauchi, M., Koshiya, S., Satoh, F., Takahashi, H., Handa, N., Murano, T., Koike, M., Imazono, T., Koeda, M., Nagano, T., Sasai, H., Oue, Y., Yonezawa, Z., Kuramoto, S., 2014. Chemical State Information of Bulk Specimens Obtained by SEM-Based Soft-X-Ray Emission Spectrometry. Microsc. Microanal. 20, 692–697. <https://doi.org/10.1017/S1431927614000439>.
- Tischendorf, G., Gottesmann, B., Forester, H.J., Trumbull, R.B., 1997. On Li-bearing micas: estimating Li from electron microprobe analyses and improved diagram for graphical representation. Mineral. Mag. 61, 809–834.
- Tischendorf, G., Forester, H.J., Gottesmann, B., 1999. The correlation between lithium and magnesium in trioctahedral micas: improved equation for Li₂O estimation from MgO data. Mineral. Mag. 63, 57–74.
- Van Velthuizen, J., Chao, G.Y., 1989. Griceite, LiF, a new mineral species from Mont Saint-Hilaire, Quebec. Can. Mineral. 125–127.
- Xiaobing, L., Holland, J., Burgess, S., Bhadare, S., Yamaguchi, S., Birtwistle, D., Statham, P., Rowlands, N., 2013. Detection of Lithium X-rays by EDS. Microsc. Microanal. 19, 1136–1137. <https://doi.org/10.1017/S1431927613007678>.
- Yamamoto, Y., Morita, H., Yamada, H., Takahashi, H., Takakura, M., Kikuchi, N., Nokuo, T., Erdman, N., 2016. The Study of "Window-less" EDS Detector with Low Voltage FE-SEM. Microsc. Microanal. 22, 640–641. <https://doi.org/10.1017/S1431927616004050>.
- Yamamoto, Y., Murano, T., Onodera, H., Erdman, N., Matsuda, R., Matsuda, A., 2020. Time Resolved SEM-SXES Analysis for Lithium Material. Microsc. Microanal. 26, 68–70. <https://doi.org/10.1017/S1431927620013276>.
- Yavuz, F., 2001. LIMICA: a program for estimating Li from electron-microprobe mica analyses and classifying trioctahedral micas in terms of composition and octahedral site occupancy. Comput. Geosci. 27, 215–227.
- Yelatontsev, D., Mukhachev, A., 2021. Processing of lithium ores: Industrial technologies and case studies – a review. Hydrometallurgy 201, 105578. <https://doi.org/10.1016/j.hydromet.2021.105578>.
- Zeng, G., Liu, Y., Chen, D., Zhen, C., Han, Y., He, W., 2021. Natural Lepidolite Enables Fast Polysulfide Redox for High-Rate Lithium Sulfur Batteries. Adv. Energy Mater. 11, 2102058. <https://doi.org/10.1002/aem.202102058>.
- Zschornack, G., 2007. Handbook of X-Ray Data. Springer.